

# SANDIA REPORT

SAND97-0159 • UC-122

Unlimited Release

Printed April 1997

## Fluid Permeability of Deformable Fracture Networks

Stephen R. Brown, Ronald L. Bruhn

RECEIVED

APR 29 1997

OSTI

Prepared by  
Sandia National Laboratories  
Albuquerque, New Mexico 87185 and Livermore, California 94550

Sandia is a multiprogram laboratory operated by Sandia Corporation, a Lockheed Martin Company, for the United States Department of Energy under Contract DE-AC04-94AL85000.

DISTRIBUTION OF THIS DOCUMENT IS UNLIMITED

Approved for public release; distribution is unlimited



Sandia National Laboratories



MASTER

Issued by Sandia National Laboratories, operated for the United States Department of Energy by Sandia Corporation.

**NOTICE:** This report was prepared as an account of work sponsored by an agency of the United States Government. Neither the United States Government nor any agency thereof, nor any of their employees, nor any of their contractors, subcontractors, or their employees, makes any warranty, express or implied, or assumes any legal liability or responsibility for the accuracy, completeness, or usefulness of any information, apparatus, product, or process disclosed, or represents that its use would not infringe privately owned rights. Reference herein to any specific commercial product, process, or service by trade name, trademark, manufacturer, or otherwise, does not necessarily constitute or imply its endorsement, recommendation, or favoring by the United States Government, any agency thereof, or any of their contractors or subcontractors. The views and opinions expressed herein do not necessarily state or reflect those of the United States Government, any agency thereof, or any of their contractors.

Printed in the United States of America. This report has been reproduced directly from the best available copy.

Available to DOE and DOE contractors from  
Office of Scientific and Technical Information  
P.O. Box 62  
Oak Ridge, TN 37831

Prices available from (615) 576-8401, FTS 626-8401

Available to the public from  
National Technical Information Service  
U.S. Department of Commerce  
5285 Port Royal Rd  
Springfield, VA 22161

NTIS price codes  
Printed copy: A03  
Microfiche copy: A01

**DISCLAIMER**

**Portions of this document may be illegible  
in electronic image products. Images are  
produced from the best available original  
document.**

SAND97-0159  
Unlimited Release  
Printed April 1997

Distribution  
Category UC-122

## Fluid Permeability of Deformable Fracture Networks

Stephen R. Brown\*  
Geomechanics Department  
Sandia National Laboratories  
Albuquerque, New Mexico 87185-0751

Ronald L. Bruhn  
Department of Geology and Geophysics  
University of Utah  
Salt Lake City, Utah 84112-1183

---

\*Now at Applied Research Associates, RR 1 Box 120 A, Waterman Road, South Royalton, Vermont 05068

## Fluid Permeability of Deformable Fracture Networks

Stephen R. Brown\*  
Geomechanics Department  
Sandia National Laboratories  
Albuquerque, New Mexico 87185-0751

Ronald L. Bruhn  
Department of Geology and Geophysics  
University of Utah  
Salt Lake City, Utah 84112-1183

### Abstract

We consider the problem of defining the fracture permeability tensor for each grid lock in a rock mass from maps of natural fractures. For this purpose we implement a statistical model of cracked rock due to M. Oda [1985], where the permeability tensor is related to the crack geometry via a volume average of the contribution from each crack in the population. In this model tectonic stress is implicitly coupled to fluid flow through an assumed relationship between crack aperture and normal stress across the crack. We have included the following enhancements to the basic model: (1) a realistic model of crack closure under stress has been added along with the provision to apply tectonic stresses to the fracture system in any orientation. The application of stress results in fracture closure and consequently a reduction in permeability. (2) The fracture permeability can be superimposed onto an arbitrary anisotropic matrix permeability. (3) The fracture surfaces are allowed to slide under the application of shear stress, causing fractures to dilate and result in a permeability increase. Through an example we demonstrate that significant changes in permeability magnitudes and orientations are possible when tectonic stress is applied to a fracture system.

---

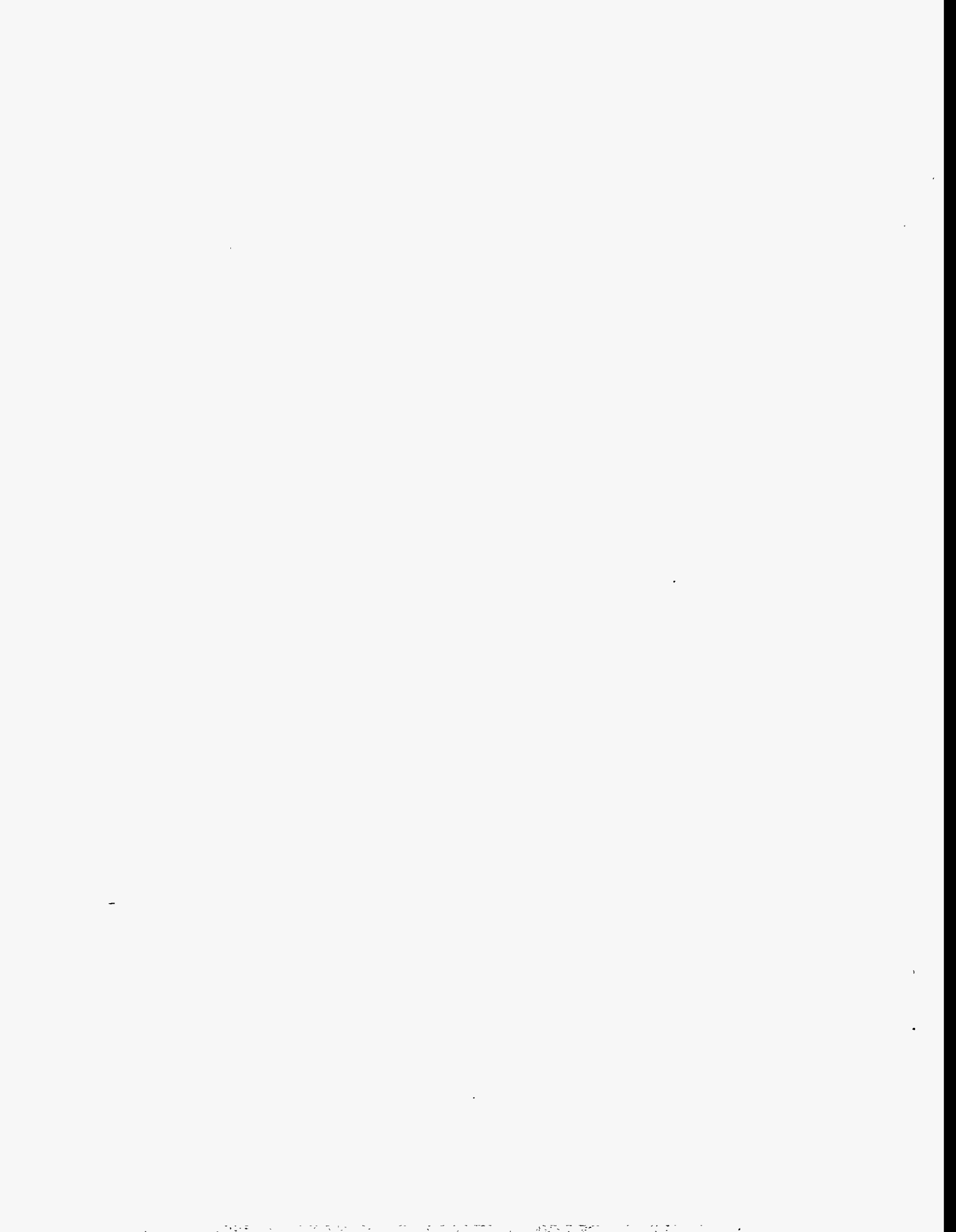
\*Now at Applied Research Associates, RR 1 Box 120 A, Waterman Road, South Royalton, Vermont 05068

# Contents

<b>1</b>	<b>Introduction</b>	<b>7</b>
<b>2</b>	<b>Oda's Model</b>	<b>7</b>
2.1	Fabric Tensor	7
2.2	Elastic Compliance	8
2.3	Fluid Permeability	8
<b>3</b>	<b>Deformation-dependent Fracture Permeability</b>	<b>10</b>
3.1	Surface Roughness Effects	10
3.2	Description of Surface Roughness	11
3.3	Fracture Closure under Normal Stress	12
3.4	Dilation Due To Shear Sliding	12
3.5	Amount of Fracture Slip	13
<b>4</b>	<b>Revised Model and Application</b>	<b>14</b>
4.1	Example Application	14
<b>5</b>	<b>Summary and Conclusions</b>	<b>15</b>
<b>6</b>	<b>Acknowledgments</b>	<b>15</b>
<b>7</b>	<b>References</b>	<b>16</b>
<b>A</b>	<b>Software</b>	<b>A1</b>
A.1	oda2d.m	A1
A.2	dperm.m	A7
A.3	getangle.m	A8
A.4	lambfit.m	A9
A.5	polvect.m	A10
A.6	slipopen.m	A11
A.7	walsh.m	A12
<b>B</b>	<b>Distribution</b>	<b>B1</b>
	External	B1
	Internal	B2

## List of Figures

1	Interconnectivity parameter. . . . .	10
2	Fractured outcrop data. . . . .	16
3	Aperture distributions. . . . .	16
4	Example fabric tensor and zero-stress permeability tensor. . . . .	17
5	Permeability tensors for (5 2.5) stress. . . . .	17
6	Permeability tensors for (2.5 5) stress. . . . .	18
7	Permeability tensors for (5 1) stress. . . . .	18
8	Permeability tensors for (1 5) stress. . . . .	19
9	Permeability tensors for (5 0.5) stress. . . . .	19
10	Permeability tensors for (0.5 5) stress. . . . .	20





# 1 Introduction

The state of the art in simulation of fluid flow in fractured reservoirs relies on the application of dual porosity numerical models. These models contain two separate (possibly anisotropic) overlapping porous media, one for a permeable matrix and one for fractures in an impermeable medium. Both media are coupled so that fluid can flow from one to the other. The properties of each of the two components can vary from grid block to grid block as is typical in a finite element analysis. The fractured medium is equivalent to an anisotropic continuum with the permeability defined as if there were three mutually orthogonal regular sets of infinitely long parallel-plate fractures, with a constant spacing and aperture.

We have been considering the problem of defining approximate fracture permeability and elasticity tensors for each grid block in a fractured reservoir from maps of natural fractures. As a practical first step, we have developed a computer version of the statistical model for cracked rock due to M. Oda and coworkers [see references in the following section]. Furthermore, we have modified Oda's standard model to include some important stress- and deformation-dependent processes.

## 2 Oda's Model

In a series of papers, M. Oda and coworkers present a statistical approach to describing and modeling the elastic deformation and fluid flow properties of fractured rock [Oda, 1982; Oda, 1984; Oda, 1985; Oda, 1986; Oda, 1988; Oda et al., 1984; Oda et al., 1986; Oda et al., 1987]. In this approach, the elastic compliance and permeability properties are related to the fracture geometry through tensors. The tensors for each physical property are derived by taking a volume average of the expected effect of each fracture in the population. The volume average contains functions of the fracture orientation, length, and aperture, in such a way that long fractures or wide fractures contribute relatively more than their smaller cousins. In this model elasticity can be implicitly coupled to fluid flow through relationships between fracture aperture and normal stress across the fracture.

Oda's model is practical at the expense of rigor. As mentioned below, there are some simplifying assumptions which reduce the generality of the results. However, the model is easy to implement and retains enough of the character of real fracture populations to be a significant improvement over assuming that fractures reside in three infinitely long orthogonal sets as conceptualized in dual porosity reservoir models. A significant benefit is that the permeability tensors derived from this model can easily be translated into the proper inputs for the dual porosity models.

### 2.1 Fabric Tensor

Oda [1982] envisioned that a general geometric property of cracked rock, termed the 'fabric', determines many mechanical properties of geological materials. He developed a mathematical description, a fabric tensor, which considers the following elements of crack geometry:

**Position and density of cracks.** The position of a crack is identified by the coordinates of its centroid. The density of cracks  $\rho$  is identified as the number of crack centroids per unit volume.

**Shape and dimension of cracks.** A crack is composed of two surfaces each of which has a unit normal vector  $\mathbf{n}$  or  $(-\mathbf{n})$ . The distance between the surfaces is termed the aperture  $t$ .

Cracks are assumed to have a simple shape, such as a circle in 3-D or a rectangle in 2-D which occupies the same surface area as the real crack. The crack size is therefore specified by an equivalent diameter  $r$ .

**Orientation of cracks.** A probability density function  $E(\mathbf{n}, r, t)$  is used to describe the number of cracks with diameter in the range  $r, r + dr$  with aperture in the range  $t, t + dt$  whose unit vectors  $\mathbf{n}$  are oriented within a small solid angle  $d\Omega$ .

The fabric tensor was constructed by considering these features and averaging over all cracks in each arbitrary direction, yielding:

$$F_{ij} = \rho \frac{\pi}{4} \int_0^{t_m} \int_0^{r_m} \int_{\Omega} r^3 n_i n_j E(\mathbf{n}, r, t) d\Omega dr dt. \quad (1)$$

The factor  $\pi/4$  comes from an assumed circular geometry of each fracture in 3-D. The expression is slightly different for the case of rectangular-shaped fractures in 2-D.

*Oda* [1982] shows that the first invariant of the crack tensor is related to crack density, and the second invariant of the deviatoric part of the crack tensor is a measure of anisotropy. Furthermore, *Oda* [1982] found that the crack tensor is empirically related to the uniaxial compressive strength and porosity of cracked materials. While the crack tensor properties by *Oda* [1982] suggest some relationship to the mechanical properties, it seems that this tie was not solidified until rederivation in a later series of papers.

One of the primary simplifying assumptions in the derivation of the fabric tensor (and in the related derivations for the elastic compliance and permeability tensors introduced below) concerns the relative position of fractures. Fractures are assumed to have a random position in the network and all fractures are distributed uniformly throughout the network, as is often described by a Poisson point process. For example, the exact position of any one fracture (say a particularly long one) with respect to any other is not taken into account. Only the length, orientation, aperture, and stiffness of each fracture are retained in the calculation. Thus highly conductive clusters of fractures will not affect the *Oda* analysis, but may in reality have significant effects on fluid flow. Thus in *Oda's* model, fractures in the network can be arranged in an infinite number of different ways and still have the same mechanical and fluid flow properties.

## 2.2 Elastic Compliance

Theoretical consideration of the elastic compliance of rock-like materials containing populations of open penny-shaped cracks led *Oda et al.* [1984] to a new derivation of the same fabric tensor described above. This time, the fabric tensor was related explicitly to the elastic properties. Although consideration of the elastic compliance of open penny-shaped cracks is beyond the scope of this paper, it is worth noting that further empirical studies showed a relationship between aspects of the crack tensor and the anisotropy of acoustic wave velocities in laboratory specimens [*Oda et al.*, 1986]. This result suggests the potential to develop an inverse method to derive important aspects of fracture geometry from geophysical methods.

## 2.3 Fluid Permeability

In subsequent work, *Oda* [1985] developed a tensor model for the fluid permeability of fractured rock. A new assumption required for fluid flow in this derivation requires that the fractures are

comprised of smooth parallel plates with a constant separation or aperture  $t$ . In this case fluid flow is described by the parallel plate model, where the volumetric flow rate is proportional to the aperture raised to the third power ( $t^3$ ). The permeability tensor  $k_{ij}$  is found to be:

$$k_{ij} = \lambda (P_{kk} \delta_{ij} - P_{ij}), \quad (2)$$

where

$$P_{ij} = \rho \frac{\pi}{4} \int_0^{r_m} \int_0^{t_m} \int_{\Omega} r^2 t^3 n_i n_j E(\mathbf{n}, r, t) d\Omega dr dt. \quad (3)$$

and  $\delta_{ij}$  is the Kronecker delta function. Note the differences between the tensors  $F_{ij}$  and  $P_{ij}$  with respect to the  $r$  and  $t$  terms. In (2) and (3), the fluid permeability depends on the statistical distributions of lengths  $r$ , apertures  $t$ , orientations  $n_i$ , and density  $\rho$  of fractures in a network.

The issue of fracture interconnectivity arises in this derivation. In the cubic law for flow through a single fracture a premultiplying constant of 1/12 appears [e.g. *Iwai*, 1976]. In Oda's derivation this premultiplier is replaced by a variable  $\lambda$  ranging between 0 and 1/12 to allow for imperfect interconnectivity of multiple fractures in a network. Oda [1986] argues that since elements of the fabric tensor describe fracture density and porosity, then

$$\lambda = \lambda(F_{ij}). \quad (4)$$

Oda [1986] demonstrates the following useful relationship through an empirical analysis:

$$\lambda = \lambda(F_0, A^{(F)}), \quad (5)$$

where the first invariant  $F_0$  of the fabric tensor  $F_{ij}$  can be calculated as:

$$F_0 = \rho \frac{\pi}{4} \int_0^{r_m} r^3 f(r) dr, \quad (6)$$

and

$$A^{(F)} = (3F'_{ij}F'_{ij}) / F_0. \quad (7)$$

Here,  $F'_{ij} = F_{ij} - F_0 \delta_{ij} / 3$  is the deviatoric part of  $F_{ij}$ . These relationships are discussed at length by Oda [1986] and Oda *et al.* [1987] and are illustrated in Figure 1 (reproduced from Figure 12 of Oda *et al.* [1987]). For our purposes we use the following approximation derived from this graph:

$$\lambda = 0.0210 + 0.0017F_0, \quad (8)$$

with  $\lambda$  never exceeding the value 1/12 at large  $F_0$ .

In addition to his earlier analyses of open penny-shaped cracks, Oda [1986] discussed some new aspects of the coupling of stress and fluid flow behavior for large-scale rough-walled joints and fractures based on the empirical model of normal and shear stiffness by *Barton and Choubey* [1977]. Seeking a more physically-based model, we have replaced Oda's latter analysis of deformable fractures with our own. We strive to quantitatively relate fracture closure under normal stress and fracture slip and dilation under shear stress to the roughness of the fracture surfaces.

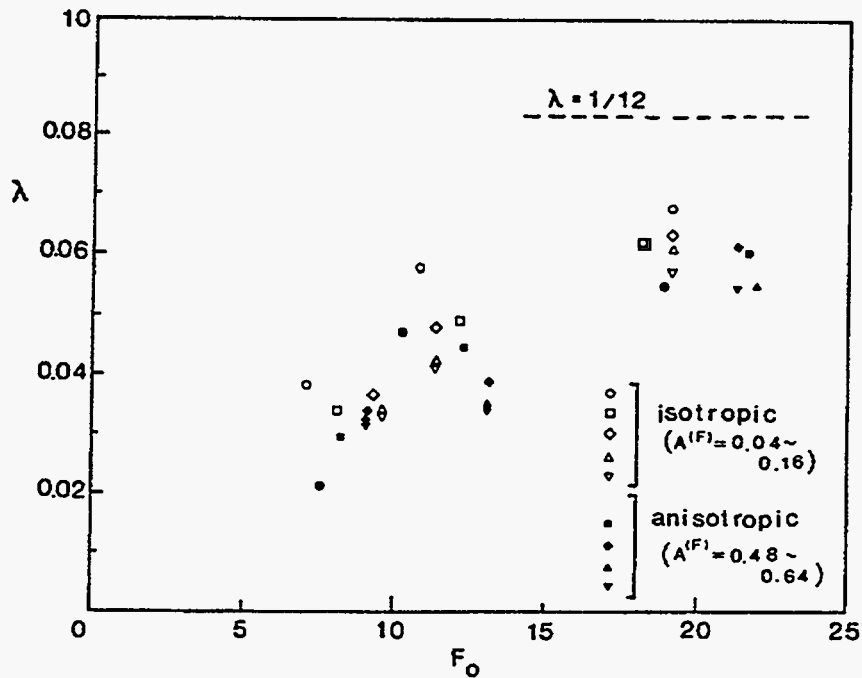


Figure 1: Relationship between the interconnectivity parameter  $\lambda$  and the first invariant of the fabric tensor  $F_0$ . Reproduced from Figure 12 of *Oda et al.* [1987].

### 3 Deformation-dependent Fracture Permeability

#### 3.1 Surface Roughness Effects

Fractures are well known for their effects on the mechanical and transport properties of rock. Mechanical properties, such as bulk elastic constants and shear strength, are strongly affected by the presence of fractures [Goodman, 1976; Brown and Scholz, 1986]. Fractures also control the fluid permeability of crystalline and tight sedimentary rock [Kranz et al., 1979; Brace, 1980]. These effects arise from the fact that the surfaces composing a fracture are rough and mismatched at some scale. The shape, size, and number of contacts between the surfaces control the mechanical properties. The surfaces are propped apart by the contacting asperities, and the resulting space between the surfaces (or aperture) controls the transport properties. Surface roughness, therefore, becomes important to quantify for the rigorous study of many fracture properties.

The parallel plate model for fluid flow can only be considered a qualitative description of flow through real fractures. Real fracture surfaces are not smooth parallel plates but are rough and contact each other at discrete points. Fluid will take a tortuous path when moving through a real fracture; thus deviations from the parallel plate model are expected. Taking the spatial variation of the aperture into consideration, laminar flow between rough surfaces has been studied theoretically, numerically, and experimentally [e.g., Walsh, 1981; Brown, 1987; Pyrak-Nolte et al., 1987; Pyrak-Nolte et al., 1988; Brown, 1989; Stesky, 1986; Zimmerman et al., 1992; Olsson and Brown, 1993]. These studies confirm that surface roughness plays an important role and can lead to a significant departure from the parallel plate model.

In our current problem we assume that the parallel plate model applies. This isn't a serious over-simplification at this stage, since it is possible to make a first-order correction for the effects of surface roughness by considering the results of *Brown* [1987], *Brown* [1989], and *Thompson and Brown* [1991]. We do, however, take advantage of the the surface roughness to determine the stress and deformation dependence of the aperture and therefore the stress and deformation effects on fluid flow.

### 3.2 Description of Surface Roughness

Measurements and analysis of surface profiles of natural fractures have established that fracture surface topography can be represented in terms of fractal geometry [*Brown and Scholz*, 1985a; *Power et al.*, 1987; *Power and Tullis*, 1991; *Power and Tullis*, 1992; *Brown*, 1995]. Topographic profiles are treated as spatial series and Fourier analysis (especially the power spectrum) is used to analyze their properties. The power spectrum is computed by breaking a time or spatial series, in this case the profile, into a sum of sinusoidal components: each with its own wavelength, amplitude, and phase. The squared amplitude of each component is referred to as its power and a plot of power versus wavenumber ( $2\pi / \text{wavelength}$ ) is referred to as the power spectrum. The phase indicates the position of the first peak of each sinusoid relative to all others. The phase spectrum is a plot of the phase as a function of wavenumber. Phase spectra for rough surfaces are typically random, that is there is no consistent relation between phase and wavenumber. The power per unit frequency interval is known as the power spectral density. Excellent introductions to spectral analysis are given by Bendat and Piersol (1971) and B ath (1974).

Linear profiles of fracture and joint surface profiles exhibit power spectral density functions of the form:

$$G(k) = Ck^{-\alpha}, \quad (9)$$

indicating self-affine fractal geometry [*Mandelbrot*, 1983]. Here,  $k$  is the wavenumber related to the wavelength  $\lambda$  according to  $k = 2\pi/\lambda$ . The exponent  $\alpha$  depends on the the fractal dimension of a surface  $D$  as  $\alpha = 7 - 2D$ . The fractal dimension of a linear profile is simply  $D_p = D - 1$ . The fractal dimension describes the proportion of high frequency to low frequency roughness and is a measure of surface texture. For natural fracture surfaces,  $D$  falls in the range  $2 \leq D \leq 3$ , with small values representing smoother surfaces. The constant  $C$  determines the standard deviation of the surface roughness about its mean plane at a particular reference profile length. Additionally, the two surfaces comprising a fracture are often closely matched at long wavelengths and mismatched at small wavelengths, resulting in an aperture distribution whose spectrum has the form (9) at small wavelengths, but flattens out at long wavelengths [*Brown and Scholz*, 1986; *Power and Tullis*, 1992; *Brown*, 1995].

*Brown* [1995] presents values of surface roughness and fractal dimensions measured at a specified profile length. We can use this information to derive the parameter  $C$  in (9). The variance in roughness of a surface  $\sigma_s^2$  at a reference length  $\lambda_0$  is derived from (9) by *Brown* [1995] as:

$$\sigma_s^2 = \int_{2\pi/\lambda_0}^{\infty} G(k)dk = \frac{C}{(\alpha - 1)} \left( \frac{\lambda_0}{2\pi} \right)^{\alpha-1}, \quad (10)$$

from which we obtain the following expression for  $C$ :

$$C = (\alpha - 1) \sigma_s^2 \left( \frac{2\pi}{\lambda_0} \right)^{\alpha-1} \quad (11)$$

### 3.3 Fracture Closure under Normal Stress

A microscopic model of contact of rough surfaces based on the studies of Hertz [see *Timoshenko and Goodier*, 1970; *Mindlin*, 1949; *Mindlin and Deresiewicz*, 1953] has been shown to successfully describe the elastic properties of a single fracture including both normal and shear stiffness [*Brown and Scholz*, 1985a; *Brown and Scholz*, 1986; *Yoshioka and Scholz*, 1989a; *Yoshioka and Scholz*, 1989b]. The surface contact model has a long history in engineering studies of friction and wear and was first presented in its present form by *Greenwood and Williamson* [1966] and first applied to rock fractures by *Walsh and Grosenbaugh* [1979]. Variations of the model have been studied by others [e.g., *Swan*, 1981; *Swan and Zongqi*, 1985].

For simplicity, we use the model of joint closure developed by *Walsh and Grosenbaugh* [1979]. In their model the fracture closure  $\delta$  depends on the standard deviation of the surface roughness  $\sigma_e$  and the compressive normal stress  $S$  as:

$$\delta = A + \sigma_e \log S, \quad (12)$$

where  $A$  is a constant depending on various roughness measures [*Brown and Scholz*, 1986]. The aperture used for fluid flow is the initial aperture  $t_0$  minus the closure due to normal stress, i.e.  $t = t_0 - \delta$ .

The surface roughness parameter  $\sigma_e$  bears some further explanation. First of all there is a distinction between the roughness of a surface  $\sigma_s$  and the effective (composite) roughness of a fracture where two surfaces are in contact  $\sigma$  [*Brown and Scholz*, 1985a; *Brown and Scholz*, 1986; *Olsson and Brown*, 1993]. The composite roughness is the negative of the aperture distribution, and its roughness  $\sigma$  is the important parameter for contact problems and fluid flow. When two mismatched surfaces with Gaussian topography are in contact, then  $\sigma \approx \sqrt{2}\sigma_s$ . Second, in the derivation of the closure law (12), contact only takes place at the upper tail of the probability distribution which describes the composite surface topography. *Walsh and Grosenbaugh* [1979] assumed that this upper tail can be approximated by an exponential distribution. The parameter  $\sigma_e$  is the standard deviation of the best-fitting exponential distribution, which is different from the standard deviation  $\sigma$  of the surface roughness as a whole. *Brown and Scholz* [1985a] give some examples of how these two roughness measures differ, and *Olsson and Brown* [1993] discuss this distinction in more detail. In very approximate terms, *Brown and Scholz* [1985a] find that  $\sigma_e \approx \sigma_s/2$  and  $A \approx \sigma_s$  for the contact of two mismatched grit-blasted glass surfaces.

### 3.4 Dilation Due To Shear Sliding

The amount of dilation or aperture increase due to the over-riding of asperities as the fracture surfaces slide past one another in shear can be estimated from the roughness characteristics following *Brown* [1995]. This can then be used to estimate the increase in permeability of each fracture in Oda's model.

For the case of two identical isotropic fractal surfaces sliding past one another in shear, a mathematical relation between aperture and offset can be found. *Brown* [1995] gives the variance of the aperture  $\sigma^2$  as:

Parameter	Description	Range	Example Problem Value
$r$	fracture length		outcrop data: Figure 2
$\theta$	fracture orientation		outcrop data: Figure 2
$t_0$	initial aperture		assumed $f(r)$ : Figure 3
$C$	scale parameter for dilation vs. slip	$4 \times 10^{-6}$ – $7 \times 10^{-3}$	$8.3 \times 10^{-6}$
$D$	fractal dimension	2.1–2.6	2.41
$\mu$	coefficient of friction	?	0.6
$F$	fraction of $r$ to determine total slip	0.01–0.001	0.001
$A$	Walsh closure model parameter	?	$t_0/3$
$\sigma_e$	Walsh closure model parameter	?	$t_0/6$

Table 1: Parameters for fracture network model. Values for the example problems were obtained as follows: The function describing initial aperture as a function of fracture length  $t_0 = f(r)$  was chosen to be linear at small  $r$  and tapering to an asymptote of about  $t_0 = 1000 \mu\text{m}$  at large  $r$  (See Figure 4). The scale factor  $C$  was calculated from equation (11) for the Austin Chalk sample "ORYX" described by *Brown* [1995]. The fractal dimension  $D$  for the same "ORYX" sample was used. A typical coefficient of friction for rock is  $\mu = 0.6$  [W.A. Olsson, personal communication]. A conservative value of the total slip parameter is  $F = 0.001$  based on results of *Cowie and Scholz* [1992]. Rough estimates of the Walsh closure model parameters were based on experimental data of *Brown and Scholz* [1985a].

$$\sigma^2 = -C \frac{\pi s^{\alpha-1} \sec(\alpha\pi/2)}{2^{\alpha-1} [\Gamma(\frac{\alpha+1}{2})]^2}. \quad (13)$$

In this expression  $s$  is the shear offset,  $\alpha$  is the scaling exponent from (9),  $\Gamma$  is the standard gamma function, and  $C$  is the scale factor from (9) and (11). Since the aperture is approximately Gaussian with standard deviation  $\sigma$ , then the mean aperture to be used for fluid flow estimates is approximately  $t = 3\sigma$  [*Brown*, 1995].

### 3.5 Amount of Fracture Slip

Frictional sliding occurs when the shear stress on the sliding plane reaches the frictional shear strength of the material. Once full sliding begins, the amount of slip cannot be determined by the stress. Total slip is controlled by external parameters such as the boundary conditions or other restrictions on the displacement. Since we consider fractures to have finite size (e.g. diameter) then slip should be limited to some small fraction of the total fracture size. If slip becomes too large, then the stress concentrations at the fracture tips will cause the fracture to grow. Since modeling of quasi-static or dynamic crack growth is beyond the scope of this work, we assume that fractures remain fixed in size regardless of the stress.

Empirical relationships have been found which show that the slip along finite-size faults are proportional to the total fault length [*Cowie and Scholz*, 1992]. This proportionality constant is typically between 0.01 and 0.001. In our modeling we assume that if the shear stress exceeds the frictional strength, then the surfaces will always slip the maximum amount as prescribed by this linear relationship.

## 4 Revised Model and Application

We have developed an extended version of Oda's model for fluid permeability of fracture networks taking into account the aforementioned stress-dependent properties of rough fractures. We consider the effect on permeability of fracture closure under normal stress and frictional sliding and resultant dilation of fractures under shear stress. A 2-dimensional version of this model has been coded in the Matlab programming language (see Appendices). The code performs the following basic steps:

1. Input fracture orientations and lengths from data file.
2. Input or choose the unstressed hydraulic aperture for each fracture.
3. Input surface roughness parameters and maximum frictional slip for each fracture.
4. Input the *in situ* stress tensor.
5. Input the rock matrix permeability tensor.
6. Compute shear stress and normal stress on each fracture by tensor transformations.
7. Check whether the shear stress on each fracture is greater than the frictional shear strength. If so, slip the fracture surfaces the maximum amount allowed and compute a new aperture based on the slip-dilation relationship (Equation (13)).
8. Close each fracture due to normal stress across the fracture (Equation (12)).
9. Compute fabric and permeability tensors from Oda's model (Equations (1)–(8)).
10. Superimpose the matrix permeability onto the fracture permeability.

The computer codes implementing these steps are given in the appendices.

### 4.1 Example Application

We illustrate the potential of this model for modeling fluid flow in fractured media through an example. It will be apparent that the stress-dependent effects are pronounced and should not be ignored in reservoir modeling.

A photograph of a large-scale fractured outcrop in the Frontier Formation, Wyoming was chosen for analysis from *Lorenz and Laubach* [1994]. The photograph was scanned with a computer and cropped to a  $350 \times 350$  pixel region representing an area of approximately  $150 \times 150$  meters. The length and orientation of the major fractures visible in this region were then digitized for analysis (see Figure 2). The numerical values of the other parameters needed for the analysis of this fracture pattern are given in Table 1. An important, yet unknown, parameter is the aperture of each fracture. An arbitrary, but reasonable, choice was made that the aperture should increase in some proportion to the fracture length, but reach a maximum value for fractures greater than a certain size (see Figure 3 for the distribution chosen).

Taking this basic input data we have computed the tensors for various anisotropic stress states with slip either allowed or not. As a reference case, Figure 4 shows the fabric tensor (which is identical for all stress states) and the permeability tensor for zero tectonic stress. The numerous



fractures parallel to the  $0^\circ$  azimuth (Figure 2) dominate the initial fabric tensor and permeability. Figures 5–10 show cases of increasing stress anisotropy applied with the greatest principal stress oriented at azimuth of either  $0^\circ$  or  $90^\circ$ . Frictional sliding causes extreme changes in the permeability tensor, including both magnitude changes and rotation of the principal axes. For this example, a stress anisotropy of 2:1 results in little, if any, frictional sliding (Figures 5 and 6). As the degree of stress anisotropy increases, the number of sliding fractures increases in kind resulting in marked permeability changes (Figures 7–10).

## 5 Summary and Conclusions

We have considered the problem of defining the fracture permeability tensor for each grid block in a rock mass from maps of natural fractures. For this purpose we implemented the statistical model of cracked rock due to M. Oda [1985]. In the original model tectonic stress was implicitly coupled to fluid flow through an assumed relationship between crack aperture and normal stress across the crack. We have added the following significant enhancements to the basic model: (1) a realistic model of crack closure under stress has been added along with the provision to apply tectonic stresses to the fracture system in any orientation. The application of stress results in fracture closure and consequently a reduction in permeability. (2) The fracture permeability can be superimposed onto an arbitrary anisotropic matrix permeability. (3) The fracture surfaces are allowed to slide under the application of shear stress, allowing fractures to dilate and result in a permeability increase.

*Warpinski et al.* [1991] discuss the significant anisotropy of tectonic stresses and the large changes in stress magnitude which have occurred during the production from oil and gas reservoirs such as Ekofisk in the North Sea. Anisotropy in the principal stresses implies that significant shear stresses can exist on suitably oriented joints or faults. We have shown through an example that if slip along the joints is allowed under shear stress, then the shape and orientation of the permeability tensor can change dramatically (nearly  $90^\circ$  in some cases) from that predicted for non-deformable and non-slipping joints. Obviously then, accurate modeling of deformable fractured reservoirs will benefit from the analysis of the stress-dependence of fracture permeability that this model provides. It is especially noted that the maximum permeability direction may not coincide with the direction of the maximum horizontal in situ principal stress.

Many reservoir simulators utilize the permeability tensor calculated for a “sugar cube” fracture geometry comprised of three orthogonal sets of parallel-plate fractures [Reiss, 1980]. The spacing and aperture of these three sets of fractures describes flow in the network. The model presented in this paper also describes flow through fracture networks as a tensor property. Our new tensor description can be cast in terms of effective sugar cube parameters. This allows the properties of complex deformable fracture networks to be readily modeled with existing reservoir simulators.

## 6 Acknowledgements

Work by S. Brown was supported primarily by the Bartlesville Energy Technology Center of the U.S. Department of Energy. Supplementary funding was provided by the Morgantown Energy Technology Center, U.S. Department of Energy. The authors thank Drs. Robert E. Lemmon and Royal J. Watts of the U.S. Department of Energy for their encouragement and comments. The Matlab computer codes presented herein are based in part on codes developed by R. Bruhn under

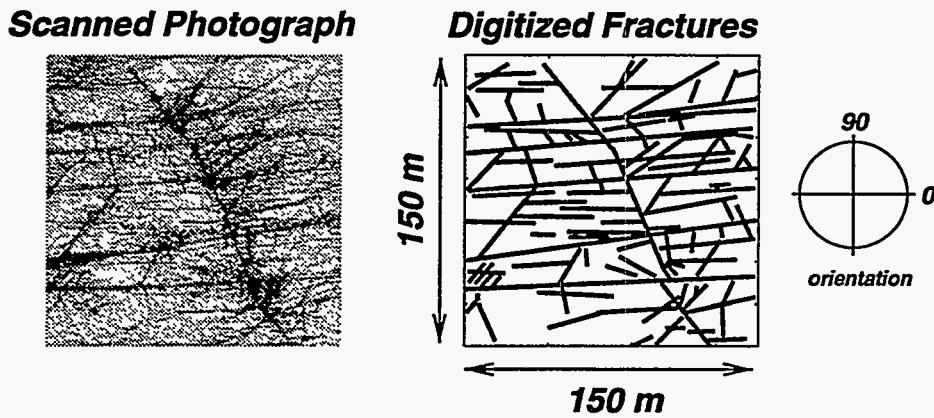


Figure 2: Fractured outcrop photograph and digitized version used for example problem. The compass defines the principal stress orientations used in the examples. From Figure 28a of *Lorenz and Laubach* [1994].

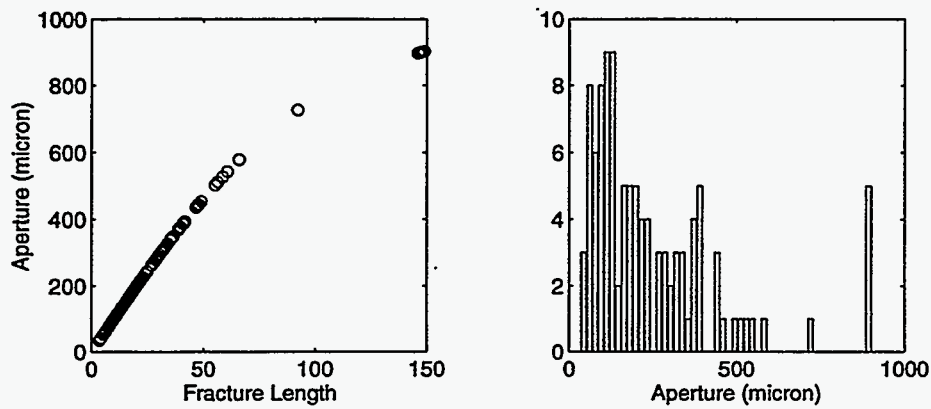


Figure 3: Aperture distributions for example problems.

contract to the Norwegian Petroleum Directorate. The original codes are available upon request to Mr. Dag Bering, Norwegian Petroleum Directorate, Professor Olav Hanssenvei 10, P.O. 600, N-4001, Stavanger, Norway.

## 7 References

- Barton, N., and V. Choubey, Shear strength of rock joints in theory and practice, *Rock Mechanics*, 10, 1-54, 1977.
- Bâth, M., *Spectral Analysis in Geophysics*, 563 pp., Elsevier, New York, 1974.
- Bendat, J. S., and A. G. Piersol, *Random Data, Analysis and Measurement Procedures*, 407 pp., John Wiley and Sons, New York, 1971.

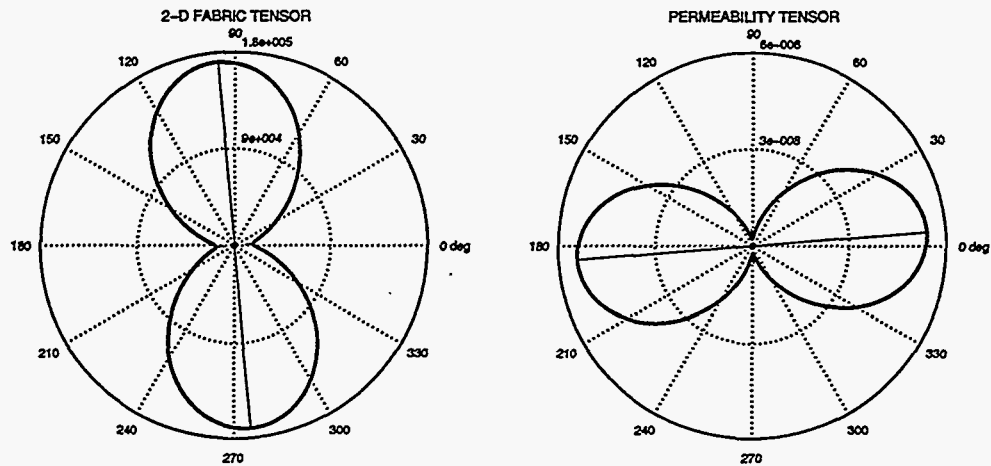


Figure 4: Left: Fabric tensor. Right: Permeability tensor for zero applied stress.

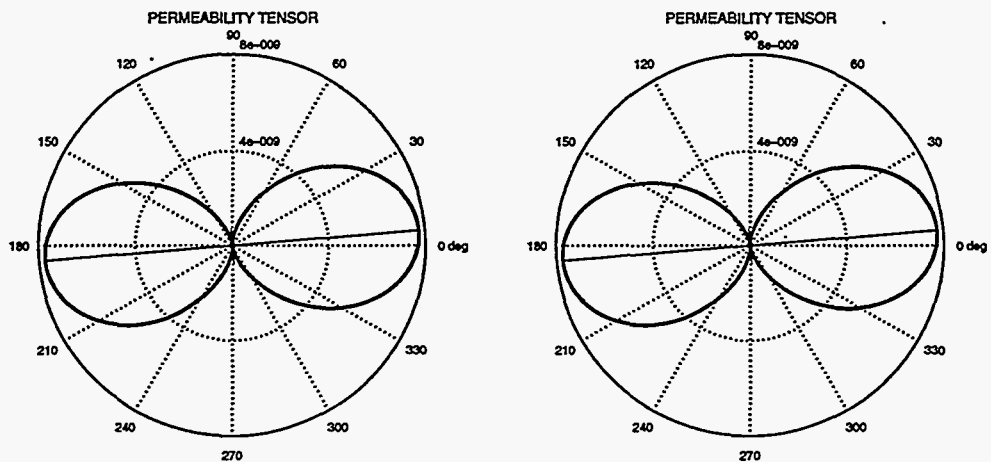


Figure 5: Left: Permeability tensor for stress [5 2.5] (5 MPa at 0° and 2.5 MPa at 90°). Slip not allowed. Right: Permeability tensor for stress [5 2.5]. Slip encouraged, but few do.

- Brace, W. F., Permeability of crystalline and argillaceous rocks, *Int. J. Rock Mech. Min. Sci. Geomech. Abstr.*, 17, 241-251, 1980.
- Brown, S. R., Fluid flow through rock joints: the effect of surface roughness, *J. Geophys. Res.*, 92, 1337-1347, 1987.
- Brown, S. R., Transport of fluid and electric current through a single fracture, *J. Geophys. Res.*, 94, 9429-9438, 1989.
- Brown, S.R. 1995. Simple mathematical model of a rough fracture. *J. Geophys. Res.* 100, 5,941-5,952.
- Brown, S.R. and C. H. Scholz, The closure of random elastic surfaces in contact, *J. Geophys. Res.*, 90, 5531-5545, 1985.
- Brown, S. R., and C. H. Scholz, Broad bandwidth study of the topography of natural rock surfaces, *J. Geophys. Res.*, 90, 12,575-12,582, 1985.
- Brown, S. R., and C. H. Scholz, Closure of rock joints, *J. Geophys. Res.*, 91, 4939-4948, 1986.

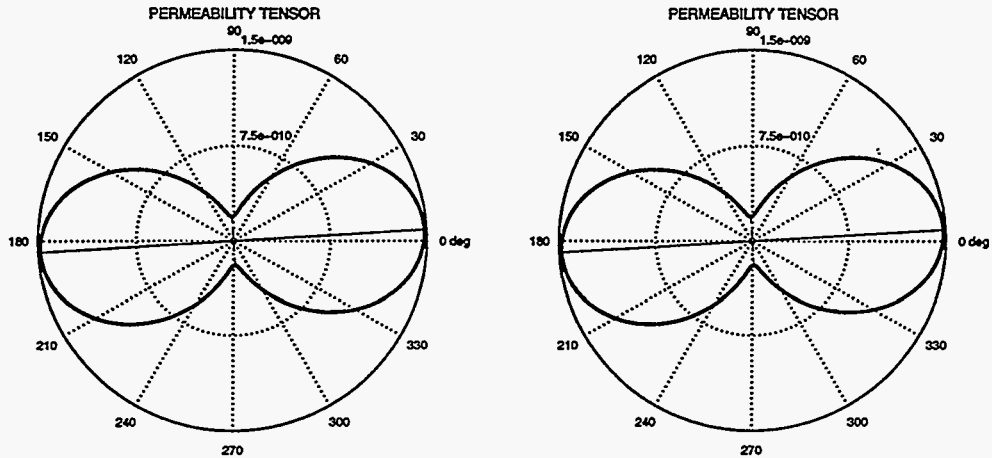


Figure 6: Left: Permeability tensor for stress [2.5 5] (2.5 MPa at 0° and 5 MPa at 90°). Slip not allowed. Right: Permeability tensor for stress [2.5 5]. Slip encouraged, but few do.

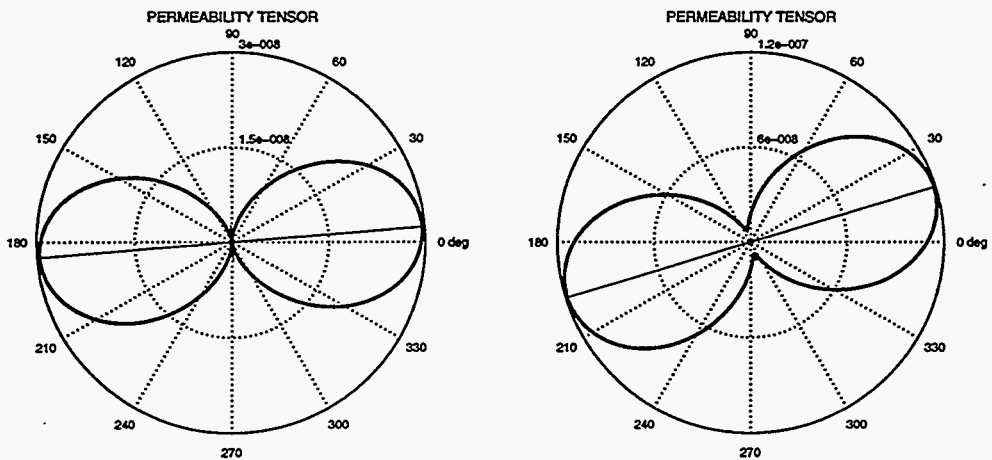


Figure 7: Left: Permeability tensor for stress [5 1] (5 MPa at 0° and 1 MPa at 90°). Slip not allowed. Right: Permeability tensor for stress [5 1]. Slip encouraged.

Cowie, P. A. and C. H. Scholz, Displacement-length scaling relationship for faults: data synthesis and discussion, *J. Struct. Geol.*, **14**, 1149-1156, 1992.

Goodman, R. E., *Methods of Geological Engineering in Discontinuous Rocks*, 472 pp., West Publishing, New York, 1976.

Greenwood, J. A., and J. Williamson, Contact of nominally flat surfaces, *Proc. R. Soc. London, A*, **295**, 300-319, 1966.

Iwai, K., *Fundamental studies of fluid flow through a single fracture*, Ph.D. thesis, Univ. of Calif., Berkeley, 1976.

Kranz, R. L., A. D. Frankel, T. Engelder, and C. H. Scholz, The permeability of whole and jointed Barre granite, *Int. J. Rock Mech. Min. Sci. Geomech. Abstr.*, **16**, 225-234, 1979.

Lorenz, J. C and S. E. Laubach, *Description and Interpretation of Natural Fracture Patterns in Sandstones of the Frontier Formation Along the Hogsback, Southwestern Wyoming*, Gas Re-

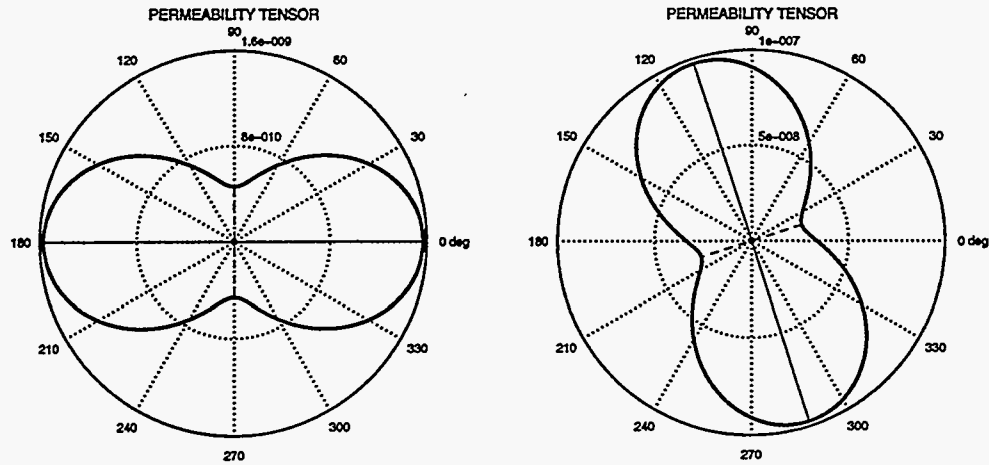


Figure 8: Left: Permeability tensor for stress [1 5] (1 MPa at 0° and 5 MPa at 90°). Slip not allowed. Right: Permeability tensor for stress [1 5]. Slip encouraged.

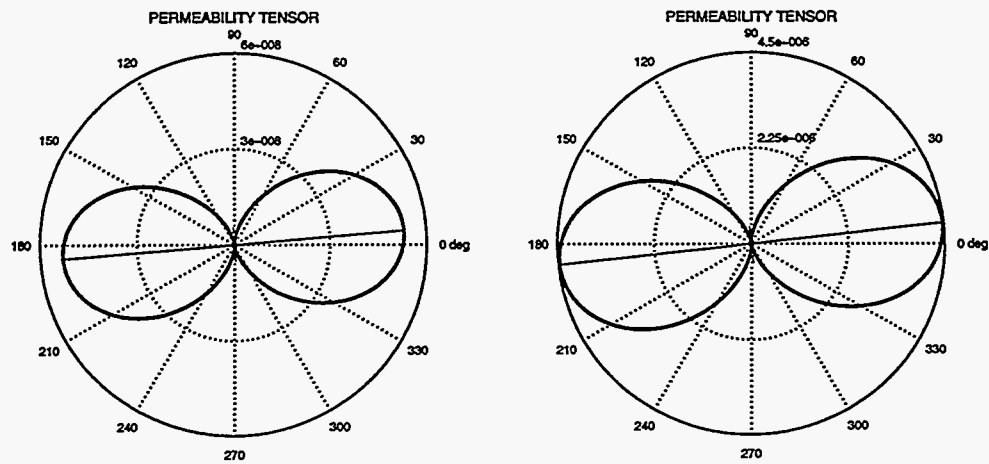


Figure 9: Left: Permeability tensor for stress [5 0.5] (5 MPa at 0° and 0.5 MPa at 90°). Slip not allowed. Right: Permeability tensor for stress [5 0.5]. Slip encouraged.

- search Institute Topical Report No. GRI-94/0020, 89 pp., 1994.
- Mandelbrot, B. B., *The Fractal Geometry of Nature*, 468 pp., W. H. Freeman, New York, 1983.
- Mindlin, R. D., Compliance of elastic bodies in contact, *J. Appl. Mech.*, *16*, 259-269, 1949.
- Mindlin, R. D. and H. Deresiewicz, Elastic spheres in contact under varying oblique forces, *J. Appl. Mech.*, *20*, 327-344, 1953.
- Oda, M., Fabric tensor for discontinuous geological materials, *Soils Fdns.*, *22*, 96-108, 1982.
- Oda, M., similarity rule of crack geometry in statistically homogeneous rock masses, *Mech. of Materials*, *3*, 119-129, 1984.
- Oda, M., Permeability tensor for discontinuous rock masses, *Geotechnique*, *35*, 483-495, 1985.
- Oda, M., An equivalent continuum model for coupled stress and fluid flow analysis in jointed rock masses, *Water Resour. Res.*, *22*, 1845-1856, 1986.
- Oda, M., An experimental study of the elasticity of mylonite rock with random cracks, *Int. J. Rock*

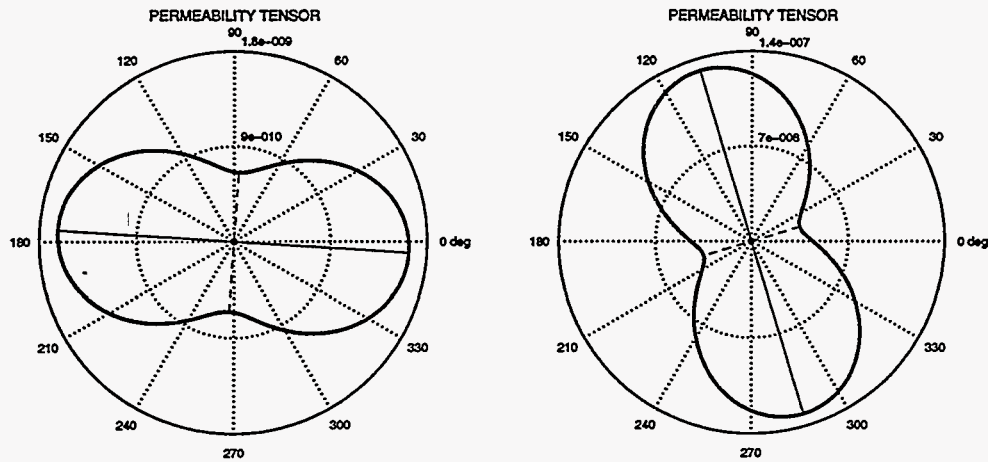


Figure 10: Left: Permeability tensor for stress [0.5 5] (0.5 MPa at 0° and 5 MPa at 90°). Slip not allowed. Right: Permeability tensor for stress [0.5 5]. Slip encouraged.

*Mech. Min. Sci. and Geomech. Abstr.*, **25**, 59-69, 1988.

- Oda, M., Y. Hatsuyama, and Y. Onishi, Numerical experiments on permeability tensor and its application to jointed granite at Stripa Mine, Sweden, *J. Geophys. Res.*, **92**, 9037-8048, 1987.
- Oda, M., K. Suzuki, and T. Maeshibu. Elastic compliance for rock-like materials with random cracks, *Soils Fdns.*, **24**, 27-40, 1984.
- Oda, M., T. Yamabe, and K. Kamemura, A crack tensor and its relation to wave velocity anisotropy in jointed rock masses, *Int. J. Rock Mech. Min. Sci. and Geomech. Abstr.*, **23**, 387-397, 1986.
- Olsson, W. A., and S. R. Brown, Hydromechanical response of a fracture undergoing compression and shear, *Int. J. Rock Mech. Min. Sci. Geomech. Abstr.*, **30**, 845-851, 1993.
- Power, W. L., and T. E. Tullis, Euclidian and fractal models for the description of rock surface roughness, *J. Geophys. Res.*, **96**, 415-424, 1991.
- Power, W. L., and T. E. Tullis, The contact between opposing fault surfaces at Dixie Valley, Nevada, and implications for fault mechanics, *J. Geophys. Res.*, **97**, 14425-15435, 1992.
- Power, W. L., T. E. Tullis, S. R. Brown, G. N. Boitnott, and C. H. Scholz, Roughness of natural fault surfaces, *Geophys. Res. Lett.*, **14**, 29-32, 1987.
- Pyrak-Nolte, L. J., Myer, L. R., Cook, N. G. W., and P. A. Witherspoon, Hydraulic and mechanical properties of natural fractures in low permeability rock, in *Proceedings of the Sixth International Congress on Rock Mechanics*, edited by G. Herget and S. Vongpaisal, pp. 225-231, A. A. Balkema, Rotterdam, Netherlands, 1987.
- Pyrak-Nolte, L. J., N. G. W. Cook, and D. D. Nolte, Fluid percolation through single fractures, *Geophys. Res. Lett.*, **15**, 1247-1250, 1988.
- Reiss, L.H., *The Reservoir Engineering Aspects of Fractured Formations*, Gulf Publishing Company, 1980.
- Stesky, R. M., Electrical conductivity of brine-saturated fractured rock, *Geophysics*, **51**, 1585-1593, 1986.
- Swan, G., Tribology and the characterization of rock joints, *Proc. U.S. Rock Mech. Symp.*, **22nd**, 402-407, 1981.
- Swan, G., and S. Zongqi, Prediction of shear behavior of joints using profiles, *Rock Mech. Rock Eng.*, **18**, 183-212, 1985.

- Thompson, M.E. & Brown, S.R. The effect of anisotropic surface roughness on flow and transport in fractures. *J. Geophys. Res.* 96, 21,923-21,932, 1991.
- Timoshenko, S. P., and J. N. Goodier, *Theory of Elasticity*, 567 pp., McGraw-Hill, New York, 1970.
- Walsh, J. B., Effect of pore pressure and confining pressure on fracture permeability, *Int. J. Rock Mech. Min. Sci. Geomech. Abstr.*, 18, 429-435, 1981.
- Walsh, J. B., and M. A. Grosenbaugh, A new model for analyzing the effect of fractures on compressibility, *J. Geophys. Res.*, 84, 3532-3536, 1979.
- Warpinski, N.R., L.W. Teufel, and D.C. Graf, Effect of stress and pressure on gas flow through natural fractures, Society of Petroleum Engineers, SPE Paper 22666, 105-118, 1991.
- Yoshioka, N., and C. H. Scholz, Elastic properties of contacting surfaces under normal and shear loads, 1, Theory, *J. Geophys. Res.*, 94, 17681-17690, 1989a.
- Yoshioka, N., and C. H. Scholz, Elastic properties of contacting surfaces under normal and shear loads, 2, Comparison of theory with experiment, *J. Geophys. Res.*, 94, 17691-17700, 1989b.
- Zimmerman, R. W., D-W. Chen, and N. G. W. Cook, The effect of contact area on the permeability of fractures, *J. Hydrol.*, 139, 79-96, 1992.

## A Software

All software is implemented in the command language of *MATLAB* (version 4), a matrix-based data analysis program published by the MathWorks, Inc., Cochituate Place, 24 Prime Park Way, Natick MA 01760.

### A.1 oda2d.m

```
function [Fdata,Kdata] = oda2d
% function [Fdata,Kdata] = oda2d

% 2-Dimensional Fabric and Permeability Tensors for fractured rock.
% Data is read from a file containing a list of fracture orientations
% and trace lengths. Aperture is computed as a function of fracture trace
% length. The matrix permeability is added to the fracture permeability
% tensor to determine total permeability.

% Written by Stephen R. Brown and Ronald L. Bruhn, 1995--1996.

clc % Clear the screen and graph, and all variables.
subplot

set(0,'DefaultAxesFontSize',12)
set(0,'DefaultTextFontSize',10)

% 2x2 kronecker delta function
kronecker = diag(ones(2,1));

% Read the fracture data file, assign variables and proceed.
filename = input('Enter data filename: ','s');
fid = fopen(filename);
data = fscanf(fid,'%g',[2 inf]);
theta = data(1,:);
diam = data(2,:);
rose([theta,theta+180]*pi/180,50);

% Enter the area of the rock face.
area = input('Enter the area of the rock mass [1.0]: ');
if isempty(area)
    area = 1;
end

c0 = input('Input parameters relating aperture to length [0 0.001 100]: ');
if isempty(c0) | (length(c0) < 3)
    c0 = [0 0.001 100]; % default: 1000 microns max; approx 900um at 100 meters
end
c0
t0 = c0(1)*ones(size(diam)) + c0(2)*tanh(diam/c0(3));

Q=input('Plot aperture distributions? [y]: ','s');
if isempty(Q)
    Q='y';
end
if Q == 'y'
    subplot(121)
    plot(diam,t0*1e6,'o')
```



```

    xlabel('Fracture Length')
    ylabel('Aperture (micron)')
    axis('square')
    subplot(122)
    hist(t0*1e6,50)
    xlabel('Aperture (micron)')
    axis('square')
    subplot
end

% Set up the stress tensor (S).
S = input('Maximum and minimum principal stresses: [0.0 0.0]: ');
if isempty(S)
    S = [0 0];
end
if size(S) == [1,1]
    S = [S S];
end
S = diag(S);

orient=input('Input orientation angle of S1 [0.0]: ');
if isempty(orient)
    orient = 0.0;
end
orient = -orient*pi/180;
aij = [cos(orient) sin(orient);-sin(orient) cos(orient)];
S = (aij*S)*aij';
S

% Enter the matrix permeability (This will be added to fracture permeability).
Kmatrix = input('Maximum and minimum matrix permeabilities: [0.0 0.0]: ');
if isempty(Kmatrix)
    Kmatrix = [0 0];
end
if size(Kmatrix) == [1,1]
    Kmatrix = [Kmatrix Kmatrix];
end
Kmatrix = diag(Kmatrix);

orient=input('Input orientation angle of K1 [0.0]: ');
if isempty(orient)
    orient = 0.0;
end
orient = -orient*pi/180;
aij = [cos(orient) sin(orient);-sin(orient) cos(orient)];
Kmatrix = (aij*Kmatrix)*aij';
Kmatrix

% Note: we assume that the thickness 'T' is 1.0 so that the
% volume of the rock mass is area*1.0.

% Compute the direction cosines of the pole to the fracture trace.
for i = 1:length(theta)
    pole = polvect(theta(i));
    np1(i) = pole(1);
    np2(i) = pole(2);
end

```

```

% Compute the four components of the two dimensional fabric tensor.
c(1,1) = sum(((diam .^2) .* np1 .* np1))/area;
c(1,2) = sum(((diam .^2) .* np1 .* np2))/area;
c(2,2) = sum(((diam .^2) .* np2 .* np2))/area;
c(2,1) = c(1,2);

% Find eigenvectors and eigenvalues of the fabric tensor.
% Note: each column of 'vectors' is an eigenvector.
[Eigenvectors,Eigenvalues] = eig(c);

% Compute the first invariant of the fabric tensor
F0 = trace(Eigenvalues);

% Compute the anisotropy index Af.
Af = abs((Eigenvalues(1,1) - Eigenvalues(2,2))/trace(Eigenvalues));

% Plot the fabric tensor axes and scale to relative magnitude
a = Eigenvalues(1,1);
b = Eigenvalues(2,2);
if (Eigenvalues(1,1) > Eigenvalues(2,2))
    n1 = Eigenvectors(1,1);
    n2 = Eigenvectors(2,1);
    m1 = Eigenvectors(1,2);
    m2 = Eigenvectors(2,2);
    F1 = Eigenvalues(1,1);
    F2 = Eigenvalues(2,2);
end
if (Eigenvalues(1,1) < Eigenvalues(2,2))
    n1 = Eigenvectors(1,2);
    n2 = Eigenvectors(2,2);
    m1 = Eigenvectors(1,1);
    m2 = Eigenvectors(2,1);
    F1 = Eigenvalues(2,2);
    F2 = Eigenvalues(1,1);
end

phi = getangle(n1,n2);

Fdata = [F1,phi,F2,F0,Af]';

% Compute the directional values of the fabric tensor.
[af,rf] = dperm(c,F1);

% Plot line in direction of maximum principal axis.
% Plot dashed line in direction of minimum principal axis.
% Set line length to 0.1 if normalized length is less than 0.1 units.
hf = [n1 -n1];
vf = [n2 -n2];
nhf = [m1 -m1];
nvf = [m2 -m2];
r = F2/F1;
if (r < 0.1),
    r = 0.1;
end

nhf = r .* nhf;

```

```

nvf = r .* nvf;

subplot
Q=input('Which subplot for F-tensor [121]: ');
if isempty(Q)
    Q=121;
end
subplot(Q)

polar(af,F1*rf)
hold on
plot(F1*hf,F1*vf,F1*nhf,F1*nvf,'--')
hold off
axis('square')

% Give the graph a title
title('2-D FABRIC TENSOR')

% Compute the P-tensor and then the permeability tensor.
% First allow joints to slip and dilate under shear stress,
% then compute the aperture using Walsh's joint closure law.

query = input('Allow slip on joints? [n]: ','s');
if isempty(query)
    query = 'n';
end
if query == 'y'
    slipstuff = input('Input slip parameters [C D mu F] = [8.3e-6 2.41 0.6 0.001]: ');
    if isempty(slipstuff)
        slipstuff = [8.3e-6 2.41 0.6 0.001];
    end
    C = slipstuff(1);
    D = slipstuff(2);
    mu = slipstuff(3);
    F = slipstuff(4);
end
for i = 1:length(t0)
    l = [np1(i) np2(i)];
    if query == 'y'
        [t1,m0] = slipopen(t0(i),diam(i),l,S,C,D,mu,F);
        wB = sqrt(m0);
        if isempty(wB)
            wB = t0(i)/3;
        end
        if isempty(t1)
            t1 = t0(i);
        end
    else
        wB = t0(i)/3;
        t1 = t0(i);
    end

    wA = wB/2;
    t(i) = walsh(t1,l,S,wA,wB);
end

```

```

disp(['Mean Aperture is ',num2str(1e6*mean(t)),' microns'])

% Compute the fracture volume.
fvol = sum((t .* diam));

% Compute the four components of the two dimensional P-tensor.
P(1,1) = sum((t.^3) .* (diam) .* np1 .* np1)/area;
P(1,2) = sum((t.^3) .* (diam) .* np1 .* np2)/area;
P(2,2) = sum((t.^3) .* (diam) .* np2 .* np2)/area;
P(2,1) = P(1,2);

% Find the value of lambda based on regression of Oda's Lambda vs F0 plot.

lambda = lambfit(F0);

% This is the computation of the permeability tensor.
% Right Hand Side - 1st term is fracture perm., 2nd is matrix permeability
KP = lambda*(trace(P)*kronecker - P) + kronecker*Kmatrix;

% Find eigenvectors and eigenvalues of the permeability tensor.
% Note: each column of 'vectors' is an eigenvector.
[Eigenvectors,Eigenvalues] = eig(KP);

% Compute the mean permeability
Km = trace(Eigenvalues)/2.0;

% ----- Plot the Permeability Tensor -----
% Plot the permeability tensor axes and scale to relative magnitude
a = Eigenvalues(1,1);
b = Eigenvalues(2,2);
if (Eigenvalues(1,1) > Eigenvalues(2,2))
    n1 = Eigenvectors(1,1);
    n2 = Eigenvectors(2,1);
    m1 = Eigenvectors(1,2);
    m2 = Eigenvectors(2,2);
    K1 = Eigenvalues(1,1);
    K2 = Eigenvalues(2,2);
end

if (Eigenvalues(1,1) < Eigenvalues(2,2))
    n1 = Eigenvectors(1,2);
    n2 = Eigenvectors(2,2);
    m1 = Eigenvectors(1,1);
    m2 = Eigenvectors(2,1);
    K1 = Eigenvalues(2,2);
    K2 = Eigenvalues(1,1);
end

phi = getangle(n1,n2);

Kdata = [K1,phi,K2,Km,fvol]';

% compute the directional permeability and prepare to graph.
[ak,rk] = dperm(KP,K1);

% Normalize principal tensor components, making maximum value equal to 1.0
% Define axes, setup plot limits and define square plot.

```

```

% Plot line of length 1.0 in direction of maximum principal axis.
% Plot dashed line, normalized length in direction of minimum principal axis.
% Set line length to 0.1 if normalized length is less than 0.1 units.
h = [n1 -n1];
v = [n2 -n2];
nh = [m1 -m1];
nv = [m2 -m2];
r = K2/K1;
if (r < 0.1), r = 0.1; end
nh = r .* nh;
nv = r .* nv;

subplot
Q=input('Which subplot for K-tensor [122]: ');
if isempty(Q)
    Q=122;
end
subplot(Q)

polar(ak,K1*rk)
hold on
plot(K1*h,K1*v,K1*nh,K1*nv,'--')
hold off
axis('square')

% Give the graph a title
title('PERMEABILITY TENSOR')

[Eigenvectors,Eigenvalues] = eig(Kmatrix);

```

## A.2 dperm.m

```
function [an,r] = dperm(KP,K1)
% function [an,r] = dperm(KP,K1)

% Calculate permeability as a function of direction.

% Written by Stephen R. Brown and Ronald L. Bruhn, 1995--1996.

an = 0:0.01:(2*pi);
r = (KP(1,1).*(cos(an).^2) + 2*KP(1,2).*cos(an).*sin(an) + ...
     (KP(2,2).*sin(an).^2))/K1;
```

### A.3 getangle.m

```
function phi = getangle(n1,n2)
% function phi = getangle(n1,n2)

% Converts direction cosines in x-y plane into angle in degrees
% measured counterclockwise from '+' x-axis.

% Written by Stephen R. Brown and Ronald L. Bruhn, 1995--1996.

% Step #1: convert from lower to upper quadrants if needed.
if (n2 < 0)
    n1 = -n1;
    n2 = -n2;
end

% Step #2: compute the angle in degrees depending on NE or NW quadrant.
if (n1 >= 0 & n2 >= 0)
    phi = acos(n1)*180/pi;
    % NE quadrant
end
if (n1 < 0 & n2 >= 0)
    phi = acos(n2)*180/pi + 90;
    % NW quadrant
end
```

#### A.4 lambfit.m

```
function [lm] = lambfit(Fo)
% function [lm] = lambfit(Fo)

% Estimate value of lambda for 2-D permeability calculation.
% note: coefficients of the equation were determined from graphs
% in paper by Oda and Hatsuyama (1987, J. Geoph. Res.). The maximum
% value for lm is 1/12 or 0.08333.

% Written by Stephen R. Brown and Ronald L. Bruhn, 1995--1996.

lm = 0.0210 + 0.0017*Fo;
if lm > 0.0833
    lm = 0.0833;
end
```



## A.5 polvect.m

```
function [p] = polvect(angle)
% function [p] = polvect(angle)

% Direction Cosine Function for Fracture Pole in 2 dimensions:
% x1 is horizontal & '+' to right, x2 is '+' vertical upwards.
% This function converts the angle of a fracture trace to a
% direction cosine of a fracture pole (90 deg. to trace).
% The output is a 1 row, 2 column vector named 'p'.
% 'angle' is measured counter clockwise from x1 axis.
% check to see which quadrant the angle is located in
% and write an error message if angle is greater than 180deg.

% Written by Stephen R. Brown and Ronald L. Bruhn, 1995--1996.

if(angle > 180)
    problem = 'angle greater than 180 deg'
    return
end

if(angle <= 90)
    % pole is located in northwest quadrant
    % change angle to radians, modify signs for fracture pole
    alpha = angle*pi/180;
    p(1) = -sin(alpha);
    p(2) = cos(alpha);
else
    % pole is located in southwest quadrant
    % modify for pole and change angle to radians.
    beta = (angle - 90)*pi/180;
    p(1) = -cos(beta);
    p(2) = -sin(beta);
end
```

## A.6 slipopen.m

```
function [t,m0] = slipopen(t0,diam,l,stress,C,D,mu,F)
% function [t,m0] = slipopen(t0,diam,l,stress,C,D,mu,F)

% Joint dilation under shear slip -- based on equation 10 of Brown,
% "Simple mathematical model of a rough fracture", JGR, 100, 5941-5952,
% 1995.

% t0 = fracture aperture before slip
% diam = fracture length
% l = direction cosines of fracture normal
% stress = stress tensor on whole system of fractures
% C = scaling factor for power spectrum of fracture roughness
% D = fractal dimension of fracture roughness for SURFACE (2<D<3)
% mu = coefficient of friction
% F = fraction of total joint length that a joint slips when the shear
% stress is high enough
% m0 = additional variance of aperture heights created by slip

% The joint dilation is 3*sqrt(m0) = three times the standard deviation
% of the NEW aperture = average NEW aperture -- NEW meaning the
% additional aperture created by slip

% Written by Stephen R. Brown and Ronald L. Bruhn, 1995--1996.

alpha = 7-2*D;

% transform stress to new axes parallel and perp to fracture
aij = [l(1) l(2);-l(2) l(1)];
stress = (aij*stress)*aij';

% Compute the normal stress
sn = stress(1,1);

% Compute the shear stress
ss = abs(stress(1,2));

% Check for slip condition
if ss >= mu*sn;
    slip = F*diam;
    denom = 2^(alpha-1) * (gamma((alpha+1)/2))^2;
    m0 = -C*(pi*slip^(alpha-1)*(1/cos(alpha*pi/2))) / denom;
    t = t0 + 3*sqrt(m0);
end
```

## A.7 walsh.m

```
function t = walsh(t0,l,stress,A,B)
% function t = walsh(t0,l,stress,A,B)

% Estimate the aperture of a crack as a function of normal stress.
% using Walsh's exponential closure law: delta = A + B*ln(sn)

% Relationships of A, and B to joint roughness and elastic
% properties are given by Brown and Scholz, "Closure of Rock Joints",
% JGR, 91, 4939-4948, 1986.

% A depends on E, nu, radius of curvature of asperities, ...
% B is essentially the standard deviation of the aperture (actually
% standard deviation of the best fitting exponential distribution of
% the upper part of the aperture distribution.

% Written by Stephen R. Brown and Ronald L. Bruhn, 1995--1996.

% Compute the normal stress
sn = l * (stress *l');

% Walsh's exponential closure law
if sn < exp(-A/B)
    closure = 0;
else
    closure = A + B*log(sn);
end
if closure > t0          % make sure we don't pinch off completely
    closure = t0 - 1.0e-6;
end

% Aperture
t = t0 - closure;
```

## DISTRIBUTION

### External:

Stephen R. Brown (30)  
Applied Research Associates  
New England Division  
RR 1 Box 120-A Waterman Road  
South Royalton, VT 05068

Greg Deitrick  
Shell Exploration & Production Company  
BTC 1136  
P. O. Box 481  
Houston, TX 77001

Nigel Higgs  
Amoco Exploration & Production  
Technology Group  
P. O. Box 3385  
Amoco Tulsa Tech Center  
4502 E. 41st St.  
Tulsa, OK 74102

Wayne Narr  
Chevron Technology Center  
P. O. Box 446  
La Habra, CA 90633-0446

Wolfgang R. Wawersik  
BES/Geosciences  
ER-15, Room E-435  
U. S. Department of Energy  
19901 Germantown Rd.  
Germantown, MD 20874-1290

Thomas Mroz (5)  
MS/E06  
U. S. Department of Energy  
Morgantown Energy Technology Center  
3610 Collins Ferry Road  
Morgantown, WV 26505

Ronald L. Bruhn (15)  
Department of Geology and Geophysics  
University of Utah  
Salt Lake City, UT 84112-1183

Peter Hennings  
Mobil Oil Company  
Exploration & Production Center  
P. O. Box 650232  
Dallas, TX 75247

Rich McMullen, Jr.  
Mobil Oil Company  
Exploration & Production Center  
P. O. Box 650232  
Dallas, TX 75265-0232

David Parrish  
CenterLine Consulting  
P. O. Box 330  
Rapid City, SD 57709

Robert E. Lemmon (15)  
U. S. Department of Energy  
Bartlesville Project Office  
P. O. Box 1398  
Bartlesville, OK 74005

Ed Parma  
Conoco, Inc.  
P. O. Box 2197, MS2016  
Houston, TX 77252-2197

Ed Novotny  
Exxon Production Research  
P. O. Box 2189  
Houston, TX 77252-2189

Bill Rizer  
Conoco Incorporated  
P. O. Box 2197  
Houston, TX 77252

Richard Chuchla  
Exxon Exploration Company  
P. O. Box 4778  
Houston, TX 77210-4778

Phil Pattillo  
Amoco Production Co.  
9425 E. 39th Street  
Tulsa, OK 74145

Dal Payne  
Chevron Production Co.  
P. O. Box 1392  
Bakersfield, CA 93302-1392

Mike Bruno  
Terralog Tech  
332 E. Foothill Blvd., Suite B  
Arcadia, CA 21006

**Internal:**

1	MS0706	D. A. Northrop (6112)
1	MS0705	J. C. Lorenz (6116)
1	MS0751	J. T. Fredrich (6117)
5	MS0751	File (6117)
1	MS0841	P. J. Hommert (9100)
1	MS0443	J. G. Arguello (9117)
1	MS0443	H. S. Morgan (9117)
1	MS0443	C. M. Stone (9117)
5	MS0899	Technical Library (4414)
1	MS9018	Central Technical Files (8940-2)
2	MS0619	Review & Approval Desk (12690) For DOE/OSTI